JACS
JOURNAL OF THE AMERICAN CHEMICAL SOCIETY

Communication

pubs.acs.org/JACS

Sol–Gel Design Strategy for Ultradispersed TiO_2 Nanoparticles on Graphene for High-Performance Lithium Ion Batteries

Wei Li,[†] Fei Wang,[†] Shanshan Feng,[†] Jinxiu Wang,[†] Zhenkun Sun,[†] Bin Li,[†] Yuhui Li,[†] Jianping Yang,[†] Ahmed A. Elzatahry,[‡,§] Yongyao Xia,[†] and Dongyuan Zhao*[,†]

[†]Department of Chemistry, Laboratory of Advanced Materials, Shanghai Key Lab of Molecular Catalysis and Innovative Materials, and State Key Laboratory of Molecular Engineering of Polymers, Fudan University, Shanghai 200433, PR China

[‡]Department of Chemistry-College of Science, King Saud University, Riyadh 11451, Saudi Arabia

[§]Advanced Technology and New Materials Research Institute, City of Scientific Research and Technology Applications, New Borg El-Arab City, Alexandria 21934, Egypt

Supporting Information

ABSTRACT: The rational design and controllable synthesis of strongly coupled inorganic/graphene hybrids represents a long-standing challenge for developing advanced catalysts and energy-storage materials. Here, we report a simple sol–gel method toward creating ultradispersed TiO_2 nanoparticles on graphene with an unprecedented degree of control based on the precise separation and manipulation of nanoparticles nucleated, grown, anchored, and crystallized and the reduction of graphene oxide (GO). The hybrid materials show ultradispersed anatase nanoparticles (~5 nm), ultrathin thickness (≤3 layers), and a high surface area of ~229 m^2/g and exhibit a high specific capacity of ~94 mA h g^{-1} at ~59 C, which is twice as that of mechanically mixed composites (~41 mA h g^{-1}), demonstrating the potential of strongly synergistic coupling effects for advanced functional systems.

Graphene, a single layer of carbon arranged in a honeycomb structure, has proved to be an exceptionally promising and versatile building block for the design of useful devises and materials because of its fascinating electronic, thermal, and mechanical properties, high specific surface areas, and easy availability from graphite.[1] Of the many graphene-based materials that have been reported, those involving inorganic nanocrystals are of particular interest because such a hybrid system has led to many promising applications in areas such as solar energy conversion, electrocatalysis, lithium ion batteries (LIBs), and so on.[2] Several methods, including the direct deposition process and a two-step strategy, have been extensively used to form inorganic nanocrystals on chemically derived graphene sheets.[3] However, one of the challenges associated with the integration is how to ensure the nucleation and growth of inorganic nanocrystals selectively on chemically derived graphene sheets over free growth in solution because it is difficult to match their compatibilities and interactions in addition to regulating the reduction of graphene oxide (GO).[4] Another challenge is how to control the particle size, uniform dispersion, and density of the loaded inorganic nanocrystals, as well as keeping the reduced graphene oxide (RGO) sheets individually separated.[5] These pose significant limitations on the creation of useful graphene-based materials.

Here, we report a versatile sol–gel strategy for the synthesis of ultradispersed TiO_2 nanoparticles on graphene, which allows precise tuning of the hybrid materials. In this case, the TiO_2 nanoparticles nucleated, grew, anchored, and crystallized on GO sheets, and the individual separation and reduction of GO sheets are precisely separated and manipulated, respectively, via a simple sol–gel process of tetrabutyl titanate (TBOT) in a pure ethanol system. The resultant TiO_2 nanocrystals/RGO sheets not only possess ultradispersed anatase nanoparticles (~5 nm), ultrathin thickness (≤3 layers), and a high surface area of ~229 m^2/g but also exhibit excellent rate capability and cycle performance as an anode material for LIBs. At ~ 59 C, a high specific capacity of ~94 mA h g^{-1} is still achieved, which is twice that of mechanically mixed TiO_2/RGO composites (~41 mA h g^{-1}).

Ultradispersed TiO_2 nanoparticles were grown on graphene sheets via a sol–gel method (Figure 1). In a typical synthesis, GO

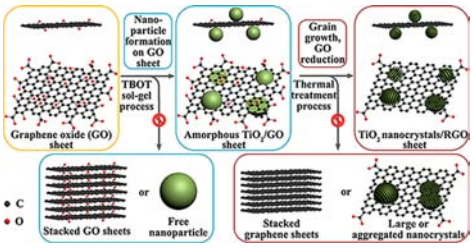

Figure 1. Schematic representation of the sol–gel design strategy toward ultradispersed TiO_2 nanocrystals on graphene.

was first prepared by a modified Hummers method,[6] and then amorphous TiO_2 nanoparticles were deposited on GO sheets via the hydrolysis and condensation of TBOT in pure ethanol with a low content of concentrated ammonia (0.1 vol %). This led to the selective formation of amorphous TiO_2/GO sheets. Followed by a thermal treatment process, amorphous TiO_2 nanoparticles crystallized into uniform anatase nanoparticles

Received: October 3, 2013
Published: November 19, 2013

dx.doi.org/10.1021/ja4100723 | J. Am. Chem. Soc. 2013, 135, 18300–18303

accompanied by the reduction of GO sheets, leading to the formation of TiO_2 nanocrystals/RGO sheets.

A field emission scanning electron microscopy (FESEM) image of the amorphous TiO_2/GO sheets (Figure 2a) shows that

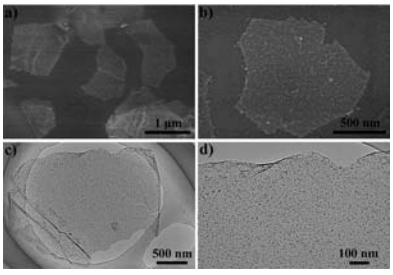

Figure 2. (a,b) FESEM and (c,d) TEM images of the amorphous TiO_2/GO sheets.

the product is composed of many free-standing and ultrathin sheets with morphology similar to that of initial GO sheets, and no naked GO sheets or free TiO_2 nanoparticles appear. A magnified FESEM image (Figure 2b) clearly reveals that a large number of TiO_2 nanoparticles with a size of ~8 nm are uniformly dispersed on the sheet. Transmission electron microscopy (TEM) images (Figure 2c,d) further disclose the ultrathin sheetlike nature and the fact that TiO_2 nanoparticles are uniformly and loosely packed on sheets. Furthermore, a high-resolution TEM (HRTEM) image clearly confirms the amorphous nature of TiO_2 nanoparticles on ultrathin GO sheets (≤3 layers) (Figure S1). These results suggest that the amorphous TiO_2 nanoparticles can be selectively loaded on GO sheets without free growth in solution. The X-ray diffraction (XRD) pattern of the amorphous TiO_2/GO sheets (Figure S2a) exhibits a weak, broad diffraction peak that can be indexed to the characteristic reflection of amorphous TiO_2. However, the typical 002 reflection at $2\theta = 11.3°$ of the initial GO sheets disappears (Figure S2b), indicating the absence of the compact layer-by-layer stacking of GO sheets in the products.[7] It further confirms that GO sheets are individually separated and uniformly coated with amorphous TiO_2 nanoparticles.

A thermal treatment of the amorphous TiO_2/GO sheets in Ar at 500 °C gives rise to the final hybrid materials. The FESEM image (Figure 3a) shows that the TiO_2 nanocrystals/RGO sheets well retain the 2D nanostructure of the parent sheets. Magnified FESEM (Figures 3b and S3) images clearly reveal that a large number of TiO_2 nanoparticles with a small particle size of ~5 nm are uniform and ultradispersed on graphene sheets. No obvious large or aggregated TiO_2 nanoparticles are visible. The XRD pattern (Figure 3c) reveals that the amorphous TiO_2 is well

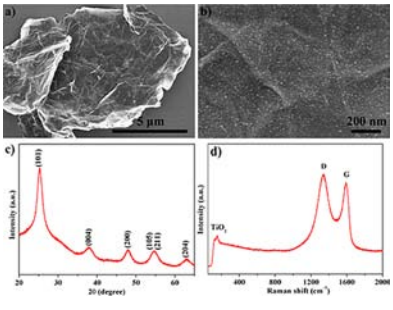

Figure 3. (a,b) FESEM images, (c) the XRD pattern, and (d) Raman spectrum of the TiO_2 nanocrystals/RGO sheets.

crystallized into anatase phase (JCPDS file no. 21-1272).[8] The average crystal size of the TiO_2 nanoparticles estimated by using Scherrer's formula is around 5 nm, which is in good agreement with the FESEM results. In addition, no diffraction peak corresponding to the restacking of graphene to form graphite can be observed, suggesting that the agglomeration of graphene sheets during the reduction process can be effectively prevented. The Raman spectrum (Figure 3d) indicates the characteristic peaks of anatase TiO_2 at 154 cm^{-1} and the D and G bands of graphene. The relative low intensity and the shift toward high frequency compared to the E_g mode at 144 cm^{-1} of bare bulk TiO_2 further illustrate the ultradispersed nature of these small TiO_2 nanoparticles and their strong interactions with the graphene support.[8a] Such strong synergistic effects would greatly promote their photocatalytic and electrical applications. The presence of C, Ti, and O elements in the sheets is also confirmed by the energy-dispersive X-ray (EDX) spectrum (Figure S4), giving ~48% graphene by mass, which is well in accordance with the TGA results (Figure S5).

TEM images (Figures 4a and S6) of the TiO_2 nanocrystals/RGO sheets also show the typical single or overlapping sheetlike

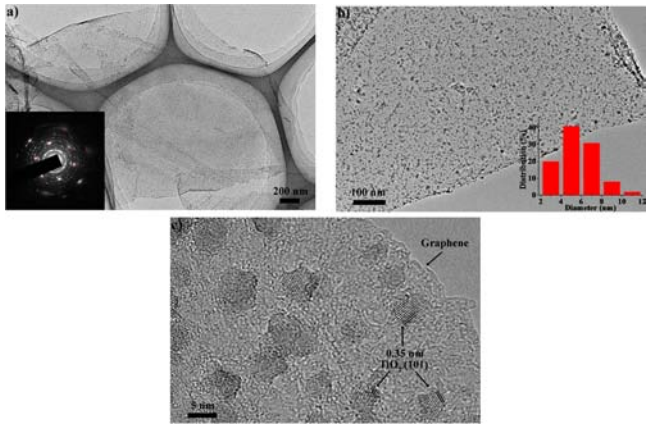

Figure 4. (a,b) TEM images of the TiO_2 nanocrystals/RGO sheets. Inset a shows the SAED pattern taken at the relatively flat edge of the sheet. Inset b is the corresponding particle size distribution of the loaded TiO_2 nanoparticles derived from 200 of TiO_2 particles in image b. (c) HRTEM image showing nanosized TiO_2 with highly exposed edges stacked on graphene sheets (one layer).

morphology but uniformly loading plenty of small nanoparticles, which is consistent with the FESEM results. The selected-area electron diffraction (SAED) pattern shows two series of well-defined diffraction patterns (Figure 4a, inset), which can be well assigned to graphene (marked with red circles)[9] and anatase TiO_2,[10] respectively, further suggesting the effective crystallization and reduction. A magnified TEM image (Figure 4b) reveals that a large number of TiO_2 nanoparticles are ultradispersed on graphene sheets. The size distribution curve of the TiO_2 nanoparticles displays a mean diameter centered at ~5 nm with a standard deviation of about 10% (Figure 4b, inset). The HRTEM image (Figure 4c) shows that highly crystalline TiO_2 nanoparticles are randomly distributed on two sides of graphene with different contrasts. A well-defined crystalline lattice can be identified with a d spacing of 0.35 nm corresponding to the (101) plane of anatase TiO_2.[11] Moreover, the edge of graphene (a single layer) can be clearly observed as indicated by the arrow. The homogeneous and ultradispersed nature of these small TiO_2 nanoparticles on graphene can be

dx.doi.org/10.1021/ja4100723 | J. Am. Chem. Soc. 2013, 135, 18300−18303

further confirmed by the scanning TEM (STEM) image and the corresponding element mapping images (Figure S7) of C, Ti, and O in the TiO_2 nanocrystals/RGO sheets.

N_2 sorption isotherms (Figure S8a,b) of the amorphous TiO_2/GO and freeze-dried GO sheets both show type IV curves with distinct hysteresis loops close to H3 type, which is a typical characteristic of the stacked sheetlike materials. The Brunauer–Emmett–Teller (BET) surface area of the amorphous TiO_2/GO sheets is calculated to be ~287 m^2/g, which is much higher than that of freeze-dried GO sheets (~215 m^2/g). It further suggests that the GO sheets are individually separated and well coated with TiO_2 nanoparticles without the compact stacking structure during the sol–gel process. After annealing in Ar at 500 °C, the resultant TiO_2 nanocrystals/RGO sheets retain the type IV curve and H3 type hysteresis loop (Figure S8c), showing a slight decrease in the BET surface area of ~229 m^2/g, which is still very high and superior to that of most of the previously reported TiO_2/RGO hybrid materials.[2c−e,12] Such high surface areas provide more surface-active sites and make the charge-carrier transport easier, leading to an enhancement of the photocatalytic and electrical performance. The slight decrease in the surface area results from the densification of amorphous TiO_2 networks and the grain growth of TiO_2 nanoparticles.[13] It is worth noting that the RGO sheets from pure GO sheets shows a low BET surface area of ~15 m^2/g (Figure S8d). It also demonstrates that the loaded TiO_2 nanoparticles can effectively prevent the agglomerations of graphene sheets during the thermal reduction process.

In this sol–gel design strategy, the unprecedented control of the hybrid materials is achieved by the rational separation and precise manipulation of the synthesis processes (involving TiO_2 nanoparticles nucleated, grown, anchored, and crystallized on GO sheets and the individual separation and reduction of GO) (Figure 1). In ethanol, GO sheets can be nearly completely exfoliated and well dispersed without restacking and fully expose the surface areas of the sheets.[4] Therefore, in the first sol–gel process, the nucleation and growth of amorphous TiO_2 nanoparticles selectively on GO sheets are preferred and can be uniformly and exclusively present at the oxygen functional group sites in the GO domain owing to their strong interactions with titanium oligomers in a covalent manner.[14] More importantly, the pure ethanol system with an ultralow content of ammonia used in this contribution results in decreasing yet well-controllable hydrolysis and condensation rates of titanium alkoxides. Thus, the heterogeneous nucleation and growth of TiO_2 on GO sheets can be preferentially achieved without the continuous/homogeneous one. Moreover, the dispersion and density of the loaded TiO_2 nanoparticles can be precisely controlled by simply tuning the ammonia content (Figure S9), which is extremely difficult in other synthetic systems. In separated thermal annealing, owing to the strong coupling effects between them, the amorphous TiO_2 nanoparticles undergo a localized crystallization on GO sheets without aggregation and migration, and GO sheets simultaneously experience a nanoparticle-protected reduction without agglomerations, which are the most important and challenging parts of other synthesis routes. Therefore, the crystallinity, phase, size, and morphology of TiO_2 nanoparticles and the reduction degree of graphene sheets can be well controlled by simply adjusting the thermal treatment temperature and atmosphere/solvent, surprisingly without changing the fascinating nanostructures (such as their ultradisperse, ultrathin nature) of the hybrid materials (Figure S10).[3e]

The lithium-insertion/extraction properties of the TiO_2 nanocrystals/RGO sheets as an anode material were investigated by galvanostatic charge/discharge measurements over a voltage range of 1.0–3.0 V. Figure 5a shows the typical charge/discharge

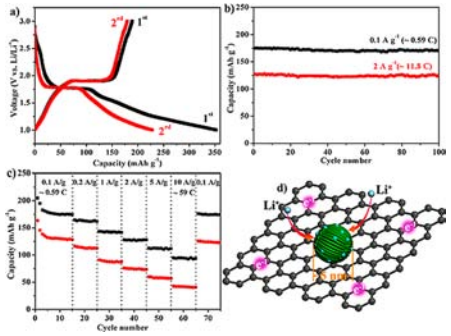

Figure 5. (a) Charge/discharge curves of the TiO_2 nanocrystal/RGO sheet electrode at a current density of 0.1 Ag^{-1} (~0.59 C). (b) Cycling performance of the TiO_2 nanocrystal/RGO sheet electrode at constant current densities of 0.1 and 2 Ag^{-1}. (c) Cycling performance of the TiO_2 nanocrystal/RGO sheet (■) and mechanically mixed TiO_2/RGO composite (red ●) electrodes at different current densities from 0.1 to 10 Ag^{-1}. All measurements were conducted within a voltage window of 1–3 V. (d) Schematic representation of the electrochemical reaction path on the TiO_2 nanocrystals/RGO sheets.

curves of a TiO_2 nanocrystal/RGO sheet electrode at a current density of 0.1 Ag^{-1} (~0.59 C), which clearly exhibits two distinct domains. The obvious horizontal discharge plateau at 1.78 V and charge plateau at 1.9 V are characteristic of lithium-insertion/extraction between tetragonal anatase TiO_2 and orthorhombic $Li_{0.5}TiO_2$.[12] Nevertheless, the slope below 1.7 V is a typical characteristic of capacitive behavior, which arises from the surface or interfacial storage of lithium ions,[2e,12] further indicating the high surface area and small particle size of TiO_2 nanocrystals on graphene sheets. As a result, a high capacity of 352 mA h g^{-1} can be derived in the first discharge, with a corresponding charge capacity of 189 mA h g^{-1} based on the weight of the TiO_2 nanocrystals/RGO sheets. Figure 5b shows the cycling performance of the hybrid sheet anode at constant current densities of 0.1 and 2 Ag^{-1}. Clearly, it shows a superior cyclic retention of 100 cycles at each current rate and a Coulombic efficiency approaching almost 100% (Figure S11). In a control experiment, free TiO_2 nanoparticles and RGO sheets are separately synthesized following the same procedures as for the synthesis of the hybrid materials without each other and then mechanically mixed together. In a voltage window of 1–3 V, the RGO sheets from the pure GO sheets have a capacity of ~151 mA h g^{-1} at a current density of 0.1 Ag^{-1} (Figure S12). The resultant TiO_2/RGO composites have a lower capacity of ~149 mA h g^{-1} in the first discharge and a poorer cycling performance than that of the TiO_2 nanocrystals/RGO sheets (Figure S13). That is because the large aggregated TiO_2 nanoparticles and restacked graphene sheets with a low surface area (15 m^2 g^{-1}) are produced in the absence of the mutual protection effects during the thermal treatment process, which leads to lower active sites for lithium storage.[15,16] In addition, the weak connections between TiO_2 nanoparticles and restacked graphene sheets are responsible for the poor cycling performance during lithium-insertion/extraction processes. The rate capabilities of the TiO_2 nanocrystals/RGO sheets and mechanically mixed TiO_2/RGO composites are then evaluated by charge/discharge at various

dx.doi.org/10.1021/ja4100723 | J. Am. Chem. Soc. 2013, 135, 18300–18303

current densities from 0.1 to 10 Ag^{-1} (Figure 5c). It is clear that the hybrid sheets show excellent cyclic capacity retention at each current density. Remarkably, a high reversible capacity of ~94 mA h g^{-1} at a current density of 10 Ag^{-1} (~59 C), which is much higher than that of mechanically mixed composites (~41 mA h g^{-1}), can still be achieved. Importantly, after the high-current-density measurements, the capacity of the TiO_2 nanocrystals/RGO sheets at 0.1 Ag^{-1} can recover to the initial value, indicating its high reversibility. The high capacity, remarkable rate capability, and outstanding cycle stability of the TiO_2 nanocrystals/RGO sheets may be caused by the synergistic coupling effects in the TiO_2 nanocrystals/RGO sheets (Figures 5d and S14):[3e,5c,17] (i) the small TiO_2 nanocrystals (~5 nm) not only greatly improve the theoretical lithium capacity ($x > 0.5$) for anatase Li_xTiO_2 but also drastically shorten the diffusion path for lithium-insertion/extraction as a result of the quantum size effect;[15] (ii) the ultrathin graphene sheets can act as a conductive substrate to improve the electron transport and present a high degree of exposure of surface or defect sites for lithium storage;[16] (iii) the unique nanostructure not only provides a high surface area for interfacial lithium storage but also maintains the integrity of the electrode during the charge and discharge processes,[8a,18] which is responsible for the high rate capability and cycling stability.

In summary, we have devised a simple and scalable sol−gel method for producing ultradisperse TiO_2 nanoparticles on graphene with a small particle size (~5 nm), ultrathin thickness (≤3 layers), and a high surface area of ~229 m^2/g. Our findings reveal that the rational separation and precise manipulation of the synthesis processes of a system (involving nanoparticles nucleated, grown, anchored, and crystallized on GO sheets and the individual separation and reduction of GO sheets) together allow unprecedented control of the hybrid materials. Furthermore, we have demonstrated that the TiO_2 nanocrystals/RGO sheets exhibit a high specific capacity of ~94 mA h g^{-1} at ~59 C, an excellent rate capability and cycle performance owing to the strong synergistic coupling effects. This sol−gel design strategy describes the blueprint of the rational design and controllable synthesis of useful graphene-based materials to extend their functions and achieve specific applications.

■ ASSOCIATED CONTENT

Ⓢ Supporting Information

Detailed experimental procedures, characterization methods, and images. This material is available free of charge via the Internet at http://pubs.acs.org.

■ AUTHOR INFORMATION

Corresponding Author

dyzhao@fudan.edu.cn

Author Contributions

W.L. and F.W. contributed equally.

Notes

The authors declare no competing financial interest.

■ ACKNOWLEDGMENTS

This work was supported by the State Key Basic Research Program of the PRC (2012CB224805 and 2013CB934104) and the NSF of China (grant no. 21210004).

■ REFERENCES

(1) (a) Geim, A. K.; Novoselov, K. S. *Nat. Mater.* **2007**, *6*, 183. (b) Stankovich, S.; Dikin, D. A.; Dommett, G. H. B.; Kohlhaas, K. M.; Zimney, E. J.; Stach, E. A.; Piner, R. D.; Nguyen, S. T.; Ruoff, R. S. *Nature* **2006**, *442*, 282. (c) Yang, X.; Cheng, C.; Wang, Y.; Qiu, L.; Li, D. *Science* **2013**, *341*, 534. (d) Chen, Z.; Ren, W.; Gao, L.; Liu, B.; Pei, S.; Cheng, H. M. *Nat. Mater.* **2011**, *10*, 424. (e) Zheng, Y.; Jiao, Y.; Ge, L.; Jaroniec, M.; Qiao, S. Z. *Angew. Chem., Int. Ed.* **2013**, *52*, 3110.

(2) (a) Liang, Y.; Li, Y.; Wang, H.; Zhou, J.; Wang, J.; Regier, T.; Dai, H. *Nat. Mater.* **2011**, *10*, 780. (b) Paek, S. M.; Yoo, E.; Honma, I. *Nano Lett.* **2009**, *9*, 72. (c) Wang, D. H.; Choi, D. W.; Li, J.; Yang, Z. G.; Nie, Z. M.; Kou, R.; Hu, D. H.; Wang, C. M.; Saraf, L. V.; Zhang, J. G.; Aksay, I. A.; Liu, J. *ACS Nano* **2009**, *3*, 907. (d) Liang, Y.; Wang, H.; Sanchez Casalongue, H.; Chen, Z.; Dai, H. *Nano Res.* **2010**, *3*, 701. (e) Yang, S. B.; Feng, X. L.; Müllen, K. *Adv. Mater.* **2011**, *23*, 3575. (f) Wu, Z. S.; Ren, W.; Wen, L.; Gao, L.; Zhao, J.; Chen, Z.; Zhou, G.; Li, F.; Cheng, H. M. *ACS Nano* **2010**, *4*, 3187. (g) Wang, H. L.; Cui, L. F.; Yang, Y. A.; Casalongue, H. S.; Robinson, J. T.; Liang, Y. Y.; Cui, Y.; Dai, H. J. *J. Am. Chem. Soc.* **2010**, *132*, 13978. (h) Wu, Z. S.; Yang, S. B.; Sun, Y.; Parvez, K.; Feng, X. L.; Müllen, K. *J. Am. Chem. Soc.* **2012**, *134*, 9082. (i) Wu, Z. S.; Sun, Y.; Tan, Y. Z.; Yang, S.; Feng, X.; Müllen, K. *J. Am. Chem. Soc.* **2012**, *134*, 19532. (j) Li, Y.; Wang, H.; Xie, L.; Liang, Y.; Hong, G.; Dai, H. *J. Am. Chem. Soc.* **2011**, *133*, 7296.

(3) (a) Wang, H.; Liang, Y.; Li, Y.; Dai, H. *Angew. Chem., Int. Ed.* **2011**, *50*, 10969. (b) Wang, H.; Robinson, J. T.; Diankov, G.; Dai, H. *J. Am. Chem. Soc.* **2010**, *132*, 3270. (c) Huang, X.; Qi, X.; Boey, F.; Zhang, H. *Chem. Soc. Rev.* **2012**, *41*, 666. (d) Xiang, Q. J.; Yu, J. G.; Jaroniec, M. *Chem. Soc. Rev.* **2012**, *41*, 782. (e) Wang, H. L.; Dai, H. J. *Chem. Soc. Rev.* **2013**, *42*, 3088.

(4) (a) Loh, K. P.; Bao, Q.; Eda, G.; Chhowalla, M. *Nat. Chem.* **2010**, *2*, 1015. (b) Dreyer, D. R.; Park, S.; Bielawski, C. W.; Ruoff, R. S. *Chem. Soc. Rev.* **2010**, *39*, 228.

(5) (a) Li, D.; Kaner, R. B. *Science* **2008**, *320*, 1170. (b) Huang, X.; Yin, Z.; Wu, S.; Qi, X.; He, Q.; Zhang, Q.; Yan, Q.; Boey, F.; Zhang, H. *Small* **2011**, *7*, 1876. (c) Liang, Y. Y.; Li, Y. G.; Wang, H. L.; Dai, H. J. *J. Am. Chem. Soc.* **2013**, *135*, 2013.

(6) Hummers, W. S.; Offeman, R. E. *J. Am. Chem. Soc.* **1958**, *80*, 1339.

(7) Chen, C.; Yang, Q.-H.; Yang, Y.; Lv, W.; Wen, Y.; Hou, P. X.; Wang, M.; Cheng, H. M. *Adv. Mater.* **2009**, *21*, 3007.

(8) (a) Li, N.; Liu, G.; Zhen, C.; Li, F.; Zhang, L. L.; Cheng, H. M. *Adv. Funct. Mater.* **2011**, *21*, 1717. (b) Li, W.; Yang, J. P.; Wu, Z. X.; Wang, J. X.; Li, B.; Feng, S. S.; Deng, Y. H.; Zhang, F.; Zhao, D. Y. *J. Am. Chem. Soc.* **2012**, *134*, 11864.

(9) Meyer, J. C.; Geim, A. K.; Katsnelson, M. I.; Novoselov, K. S.; Booth, T. J.; Roth, S. *Nature* **2007**, *446*, 60.

(10) Wang, Z.; Lou, X. W. *Adv. Mater.* **2012**, *24*, 4124.

(11) Wu, H. B.; Chen, J. S.; Lou, X. W.; Hng, H. H. *Nanoscale* **2011**, *3*, 4082.

(12) Ding, S. J.; Chen, J. S.; Luan, D. Y.; Boey, F. Y. C.; Madhavi, S.; Lou, X. W. *Chem. Commun.* **2011**, *47*, 5780.

(13) Li, W.; Deng, Y. H.; Wu, Z. X.; Qian, X. F.; Yang, J. P.; Wang, Y.; Gu, D.; Zhang, F.; Tu, B.; Zhao, D. Y. *J. Am. Chem. Soc.* **2011**, *133*, 15830.

(14) Li, W.; Zhao, D. Y. *Adv. Mater.* **2013**, *25*, 142.

(15) (a) Sudant, G.; Baudrin, E.; Larcher, D.; Tarascon, J.-M. *J. Mater. Chem.* **2005**, *15*, 1263. (b) Jiang, C.; Wei, M.; Qi, Z.; Kudo, T.; Honma, I.; Zhou, H. *J. Power Sources* **2007**, *166*, 239. (c) Borghols, W. J. H.; Lutzenkirchen-Hecht, D.; Haake, U.; van Eck, E. R. H.; Mulder, F. M.; Wagemaker, M. *Phys. Chem. Chem. Phys.* **2009**, *11*, 5742.

(16) (a) Yoo, E.; Kim, J.; Hosono, E.; Zhou, H.-S.; Kudo, T.; Honma, I. *Nano Lett.* **2008**, *8*, 2277. (b) Wang, G.; Shen, X.; Yao, J.; Park, J. *Carbon* **2009**, *47*, 2049.

(17) Wu, Z. S.; Zhou, G.; Yin, L.-C.; Ren, W.; Li, F.; Cheng, H. M. *Nano Energy* **2012**, *1*, 107.

(18) Yang, S.; Feng, X.; Wang, L.; Tang, K.; Maier, J.; Müllen, K. *Angew. Chem., Int. Ed.* **2010**, *49*, 4795.